

# The Parametric Transition of Strange Matter Rings to a Black Hole

H. Labranche<sup>1\*</sup>, D. Petroff<sup>1\*\*</sup>, M. Ansorg<sup>2\*\*\*</sup>

<sup>1</sup> Theoretisch-Physikalisches Institut, University of Jena, Max-Wien-Platz 1, 07743 Jena, Germany

<sup>2</sup> Max-Planck-Institut für Gravitationsphysik, Albert-Einstein-Institut, 14476 Golm, Germany

The date of receipt and acceptance will be inserted by the editor

**Abstract** It is shown numerically that strange matter rings permit a continuous transition to the extreme Kerr black hole. The multipoles as defined by Geroch and Hansen are studied and suggest a universal behaviour for bodies approaching the extreme Kerr solution parametrically. The appearance of a ‘throat region’, a distinctive feature of the extreme Kerr spacetime, is observed. With regard to stability, we verify for a large class of rings, that a particle sitting on the surface of the ring never has enough energy to escape to infinity along a geodesic.

**Key words** black hole; stationary and axisymmetric spacetimes; rings; numerical solutions; strange matter preprint number: AEI-2006-021

## 1 Introduction

In this paper, we consider in detail the parametric transition of a strange matter ring to a black hole. In [1,2], necessary and sufficient conditions for a quasi-stationary transition were presented and it was proved that an extreme Kerr black hole necessarily results. Using the analytic solution for the relativistic disc of dust [3], a transition to a black hole was found explicitly [4]. Transitions have also been found numerically for rings with a variety of equations of state [5,6]. Such parametric transitions to a black hole can be interpreted as a quasi-stationary collapse.

The methods we use to study parametric transitions differ from those in the above cited papers, since we here concentrate on the behaviour of

---

\* e-mail: H.Labranche@tpi.uni-jena.de

\*\* e-mail: D.Petroff@tpi.uni-jena.de

\*\*\* e-mail: mans@aei.mpg.de

multipole moments and on the appearance of a region of spacetime typical of metrics close to the extreme Kerr limit. These transitions are studied for strange matter, which is considered to be a form of matter that may be astrophysically relevant and has not been considered elsewhere for ring topologies. We restrict our attention here to ring configurations, since there is evidence suggesting that only rings and discs permit a transition to a black hole. We include in this paper a comparison with the corresponding transitions of rings governed by other equations of state.

Section 2 is devoted to a brief description of the equation of state used here to model strange matter. In Sec. 3 we define multipole moments at infinity and follow their progression as they tend to those of the extreme Kerr black hole. The appearance of a “throat region” separating the “inner” from the “outer world” is discussed in Sec. 4. In Sec. 5, we verify numerically that a particle resting on the ring’s surface is always gravitationally bound, a condition, which can be considered to be a minimal requirement for stability. We close with a short summary in Sec. 6.

Throughout this paper, units are used in which the gravitational constant  $G$  and speed of light  $c$  are equal to one.

## 2 Equation of state

Strange matter is a fluid made of up (u), down (d) and strange (s) quarks. Our equation of state (eos) to characterize strange matter is the same one described by Gourgoulhon et al. [7], who studied the properties of axially symmetric, stationary, spheroidal strange matter configurations. Based on the MIT bag model, we consider equal numbers of massless, non-interacting u,d,s quarks, confined to a given volume, i.e. enclosed in a “bag”. The limits of the bag correspond in our case to the surface of the star, such that the star is entirely composed of strange matter. This model leads to a simple eos:

$$\epsilon = 3p + 4B, \quad (1)$$

where  $\epsilon$  is the energy density,  $p$  the pressure and  $B$  the bag constant, characterizing the quark confinement.

In the Newtonian limit, the pressure  $p$  is low and negligible in comparison to  $B$ , so the eos takes the form  $\epsilon = \text{constant}$ . Therefore, all the known Newtonian solutions for homogeneous bodies will be found in the Newtonian limit of the MIT bag model. Of course, a quark model of matter is not relevant in the Newtonian limit, but is taken as a limiting case of our eos. Also, like the homogeneous eos, but unlike polytropic models, the density of strange matter is discontinuous at the surface.

## 3 Multipole Moments

It has been shown in [1] that the extreme Kerr solution is the only black hole limit of rotating perfect fluid bodies in equilibrium. The extreme Kerr

black hole is characterized by the relation

$$J = \pm M^2, \quad (2)$$

where  $M$  is the mass and  $J$  the angular momentum. To study quasi-stationary transitions that lead to black holes, we use bodies with a ring topology, since spheroidal bodies do not seem to have stationary sequences that lead to black holes [8]. For spheroidal bodies, a finite upper bound is observed for  $Z_0$ , which is the relative redshift of zero angular momentum photons emitted from the surface of the body and observed at infinity. In contrast, the transition to a black hole occurs if and only if  $Z_0 \rightarrow \infty$  [2]. We explore here such transitions with the concept of multipole moments.

### 3.1 The Metric and the Definition of Multipole Moments

The line element for a stationary and axisymmetric spacetime containing a uniformly rotating fluid can be written in the form

$$ds^2 = e^{-2U} [e^{2k} (d\rho^2 + d\zeta^2) + W^2 d\varphi^2] - e^{2U} (ad\varphi + dt)^2, \quad (3)$$

where the functions  $e^{2k}$ ,  $e^{2U}$ ,  $W$  and  $a$  depend only on  $\rho$  and  $\zeta$ . The equatorial plane is given by  $\zeta = 0$  and the axis of rotation by  $\rho = 0$ .

To describe the surface of the ring, it is useful to introduce the metric potential  $V$ ,

$$e^{2V} = e^{2U} [(1 + \Omega a)^2 - \Omega^2 W^2 e^{-4U}],$$

where  $\Omega$  is the angular velocity of the fluid with respect to infinity. The function  $V$  is constant along isobaric surfaces and the surface of the ring, defined to be the surface of vanishing pressure, can thus be denoted by  $V = V_0$ . The constant  $V_0$  is related to the relative redshift  $Z_0$  via

$$e^{-V_0} - 1 = Z_0. \quad (4)$$

Consider now the vacuum region exterior to the mass distribution and extending to infinity. It is not possible to solve Einstein's equations in this region alone since the boundary conditions valid on the surface of the ring (and indeed the location of this surface) can only be found after solving the global problem. Considering the vacuum region will suffice for introducing the multipole moments however. In this region, there exists a conformal coordinate transformation  $z' = z'(z)$  ( $z' := \rho' + i\zeta'$ ,  $z := \rho + i\zeta$ ) allowing one to choose  $\rho'(\rho, \zeta) = W(\rho, \zeta)$ , which then leads to the metric

$$ds^2 = e^{-2U} [e^{2k'} (d\rho'^2 + d\zeta'^2) + \rho'^2 d\varphi^2] - e^{2U} (ad\varphi + dt)^2, \quad (5)$$

which we will use below to define the multipole moments. Note that the Cauchy-Riemann conditions for the transformation from (3) to (5) imply  $W_{,\rho\rho} + W_{,\zeta\zeta} = 0$ , which is valid only in the vacuum domain. It follows from

axial symmetry that  $W = 0$  holds for  $\rho = 0$  ( $W = \mathcal{O}(\rho)$ ). Along the axis of rotation,  $\rho = 0$ , one of the Cauchy-Riemann conditions then yields

$$\left. \frac{\partial \zeta'}{\partial \zeta} \right|_{\rho=0} = \left. \frac{\partial \rho'}{\partial \rho} \right|_{\rho=0} = \left. \frac{\partial W}{\partial \rho} \right|_{\rho=0} = \lim_{\rho \rightarrow 0} \frac{W}{\rho}. \quad (6)$$

After solving numerically for the metric functions in Eq. (3), an expansion of  $W/\rho$  along the axis of rotation then allows us to find an expansion of  $\zeta'$  in terms of  $\zeta$  and vice versa. Thus, taking into account that  $\rho = 0 \Leftrightarrow \rho' = 0$ , we are in a position to be able to write down the series expansion about the point  $\zeta' = +\infty$  for the metric functions, which will be used in defining the multipole moments (see Eq. 13).

Turning our attention back to Eq. (5), the Einstein equations governing  $a$  and  $e^{2U}$  can be rewritten using the single, complex Ernst equation

$$(\Re f) \triangle f = \nabla f \cdot \nabla f, \quad (7)$$

where  $f$  is the complex function  $f = e^{2U} + ib$ ,  $\Re f$  is the real part of  $f$  and  $\triangle$  and  $\nabla$  are respectively the Laplacian and the gradient operators in a three dimensional Euclidean space. Once  $a$  and  $U$  have been solved for, the metric function  $k'$  can be calculated via a line integral. Solutions of the Ernst equation lead to solutions of the Einstein equations and the metric potentials can be calculated from:

$$a_{,\rho'} = \rho' e^{-4U} b_{,\zeta'} \quad (8)$$

$$a_{,\zeta'} = -\rho' e^{-4U} b_{,\rho'} \quad (9)$$

$$k'_{,\rho'} = \rho' [U_{,\rho'}^2 - U_{,\zeta'}^2 + \frac{e^{-4U}}{4} (b_{,\rho'}^2 - b_{,\zeta'}^2)] \quad (10)$$

$$k'_{,\zeta'} = 2\rho' [U_{,\rho'} U_{,\zeta'} + \frac{e^{-4U}}{4} b_{,\rho'} b_{,\zeta'}]. \quad (11)$$

From the Ernst potential  $f$ , one can define another potential  $\xi$ :

$$\xi = \frac{1-f}{1+f}. \quad (12)$$

Taking the potential  $\xi$  on the positive part of the axis of rotation ( $\rho' = 0$ ,  $\zeta' > 0$ ), we can make a series expansion of it at infinity:

$$\xi(\rho' = 0, \zeta') = \sum_{n=0}^{\infty} \frac{m_n}{\zeta'^{n+1}}. \quad (13)$$

We assume reflectional symmetry about the equatorial plane in this paper for which it follows that  $m_n$  is real for even  $n$  and imaginary for odd  $n$  [9, 10].

The multipole moments  $P_n$  defined by Geroch [11] and Hansen [12] are algebraic combinations of the coefficients  $m_n$  and characterize the Ernst

potential uniquely. In this article, we consider the 7 first multipole moments of the infinite set given in [13] as

$$P_j = m_j \quad \text{for } j = 0, 1, 2, 3 \quad (14a)$$

$$P_4 = m_4 - \frac{1}{7}M_{20}m_0 \quad (14b)$$

$$P_5 = m_5 - \frac{1}{3}M_{30}m_0 + \frac{1}{21}M_{20}m_1 \quad (14c)$$

$$P_6 = m_6 + \frac{1}{33}M_{20}m_0^3 - \frac{5}{231}M_{20}m_2 + \frac{4}{33}M_{30}m_1 - \frac{8}{33}M_{31}m_0 - \frac{6}{11}M_{40}m_0, \quad (14d)$$

where  $M_{jk} \equiv m_j m_k - m_{j-1} m_{k+1}$ . We point out that  $P_0 = M$  and  $P_1 = iJ$  always hold. The multipoles  $P_n$  can then be normalized as follows:

$$y_n = i(-2i\Omega)^{n+1} P_n. \quad (15)$$

For the Kerr black hole, the multipole moments are simply

$$P_n^{(Kerr)} = M(iJ/M)^n, \quad (16)$$

where  $M$  and  $J$  are respectively the mass and the angular momentum of the black hole. Using the relation

$$J = \frac{4\Omega_H M^3}{1 + 4\Omega_H^2 M^2}, \quad (17)$$

where  $\Omega_H$  is the angular velocity of the horizon, we then find

$$y_n^{(Kerr)}(y_0) = y_0 \left( \frac{2y_0^2}{1 + y_0^2} \right)^n. \quad (18)$$

Through this normalization, all multipoles  $y_n$  of the extreme Kerr black hole are equal to one, as can be seen by taking into account  $y_0 = 2\Omega_H M = 1$ .

### 3.2 Multipole Moments of Rings

As  $V_0$  tends to  $-\infty$ , we expect the multipole moments to become closer and closer to those of an extreme Kerr black hole. We tested this numerically by making use of a (slightly modified version of a) highly accurate computer program as described in [14]. This program was used for all the results presented in this paper. Since the  $n^{\text{th}}$  multipole moment requires the calculation of  $n+1$  derivatives, which results in a loss of accuracy, we could not calculate arbitrarily many numerically.

Figures 1 and 2 show the first seven multipole moments for homogeneous and strange matter rings where the ratio between the inner coordinate radius  $\rho_i$  and the outer radius  $\rho_o$  (see Fig. 3) is held constant at a value of  $\rho_i/\rho_o = 0.7$ . The left side of the plots corresponds to the Newtonian limit

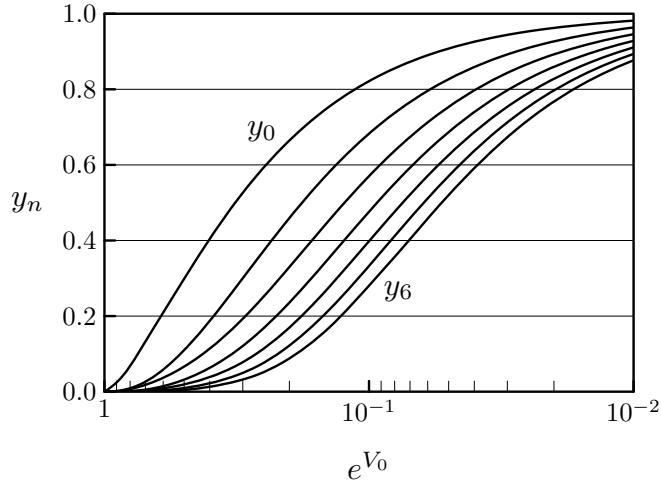


**Fig. 1** The normalized multipoles  $y_n$  versus  $e^{V_0}$  for homogeneous rings with  $\rho_i/\rho_o = 0.7$ .

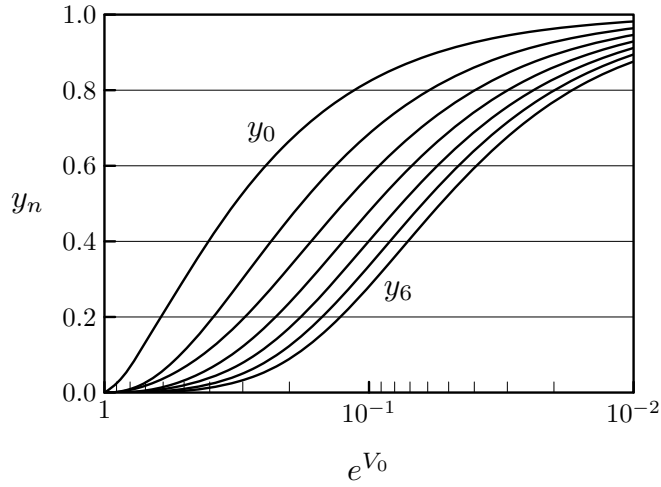


**Fig. 2** The normalized multipoles  $y_n$  versus  $e^{V_0}$  for strange matter rings with  $\rho_i/\rho_o = 0.7$ .

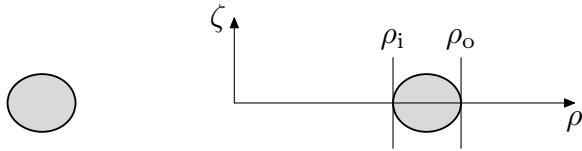


**Fig. 3** Example of a meridional cross-section of a strange matter ring. The ring in this example has the parameters  $\rho_i/\rho_o = 0.7$  and  $e^{2V_0} = 0.1$ .

and the right side tends toward the black hole limit. As  $V_0 \rightarrow -\infty$ , the normalized multipoles all tend to one, demonstrating that this sequence indeed approaches the extreme Kerr solution.

It is interesting to note, with respect to  $e^{V_0}$  (or  $Z_0$ ), how slowly the exterior spacetime approaches that of a Kerr black hole. Consider, for example, the configuration from Fig. 2 with  $e^{V_0} = 10^{-2}$ . Whereas the value  $J/M^2 = 1.00014$  is very close to the limiting value of one reached in the extreme Kerr limit, the product  $2\Omega M = 0.9813$  deviates rather significantly from it. This makes itself felt particularly for the higher multipole moments where powers of  $\Omega$  are in play. The moment  $y_4$ , for example, has reached only a value of  $y_4 \approx 0.91$  for this configuration.

To understand better the nature of the transition to the black hole, we compare the multipole moments of the above strange matter ring sequence with those of the Kerr solution. In Fig. 4 the  $y_n$  for  $n = 1 \dots 6$  are plotted against  $y_0 = 2\Omega M$  for the strange matter ring sequence from above. A corresponding picture for the sequence of Kerr solutions (see (18)) is displayed in Fig. 5. The clear similarity between these plots is emphasized in Fig. 6 where each  $y_n$  for the ring (solid line) and the Kerr solution (dotted line) is compared in a small figure over its whole range. The region very close to the extreme Kerr limit is then shown for  $y_1$ – $y_5$  in detail. The graphs strongly suggest that the slopes

$$\frac{dy_n}{dy_0}(y_0 = 1) \quad (19)$$

are the same for the Kerr family and for the strange matter ring sequence discussed here. In fact, we found these slopes to be independent of the specific eos being used.<sup>1</sup> For the Kerr solutions, it follows from (18) that

$$\frac{dy_n}{dy_0}(y_0 = 1) = n + 1, \quad (20)$$

which leads us to the conjecture that (20) holds true for all sequences of rotating bodies that admit the transition to an extreme Kerr black hole. This conjecture provides a universal growth rate with which the  $y_n$  approach unity. It would be interesting to test this conjecture for the analytically known rigidly rotating disc of dust and work in this direction is ongoing.

In Table 1, a comparison of the values of the first five moments  $y_n$  for a variety of configurations all with  $e^{V_0} = 10^{-2}$  is provided. The set of configurations chosen includes rings with various different eos and various radius ratios and also includes the uniformly rotating disc of dust. A discussion of the multipoles of this last configuration as well as plots analogous to Fig. 2 can be found in [15]. Since all multipole moments tend to one in the limit  $V_0 \rightarrow -\infty$ , these multipoles will provide almost no way of distinguishing between various configurations close to this limit.

---

<sup>1</sup> We checked this for ring sequences governed by homogeneous, polytropic and Chandrasekhar eos as well as for the rigidly rotating dust family. The Chandrasekhar eos describes a completely degenerate, zero temperature, relativistic Fermi gas.

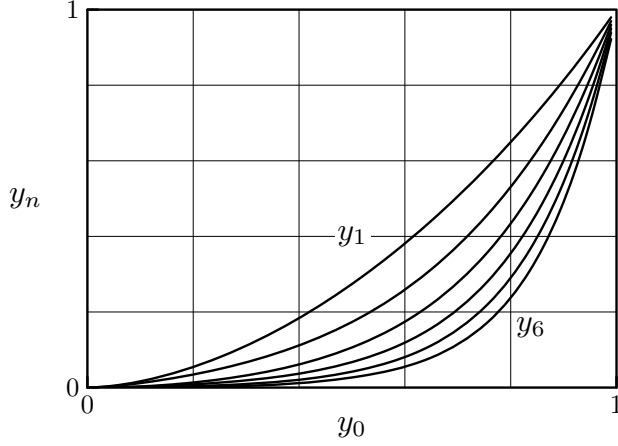


**Fig. 4** The multipole moments  $y_n$ ,  $n = 1 \dots 6$  versus  $y_0$  for strange matter rings with  $\rho_i/\rho_o = 0.7$ .

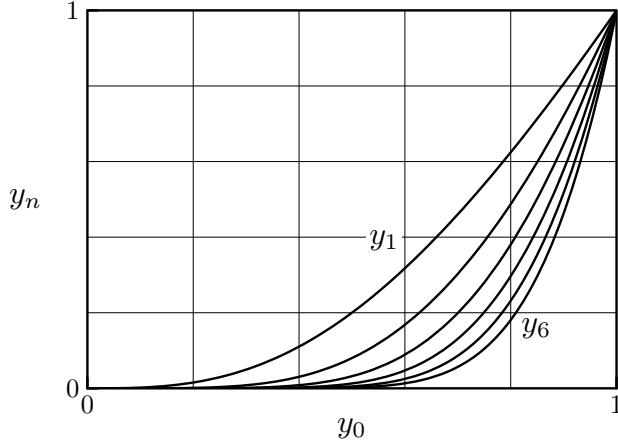


**Fig. 5** The multipole moments  $y_n$ ,  $n = 1 \dots 6$  versus  $y_0$  for the sequence of Kerr solutions.

	$y_0$	$y_1$	$y_2$	$y_3$	$y_4$
s.m. ( $r_i/r_o = 0.6$ )	0.982	0.964	0.947	0.930	0.913
s.m. ( $r_i/r_o = 0.7$ )	0.981	0.963	0.945	0.928	0.910
s.m. ( $r_i/r_o = 0.8$ )	0.981	0.962	0.943	0.925	0.907
hom. ( $r_i/r_o = 0.7$ )	0.981	0.963	0.945	0.927	0.910
pol. ( $r_i/r_o = 0.7$ )	0.982	0.965	0.948	0.931	0.914
rel. disc of dust	0.984	0.969	0.953	0.938	0.924

**Table 1** The multipole moments  $y_n$  for various configurations, all with  $e^{V_0} = 10^{-2}$ . The abbreviation ‘s.m.’ refers to a strange matter ring, ‘hom.’ to a homogeneous ring, ‘pol.’ to a polytropic ring with the polytropic index  $n = 1$  and ‘rel. disc of dust’ to the relativistic disc of dust.



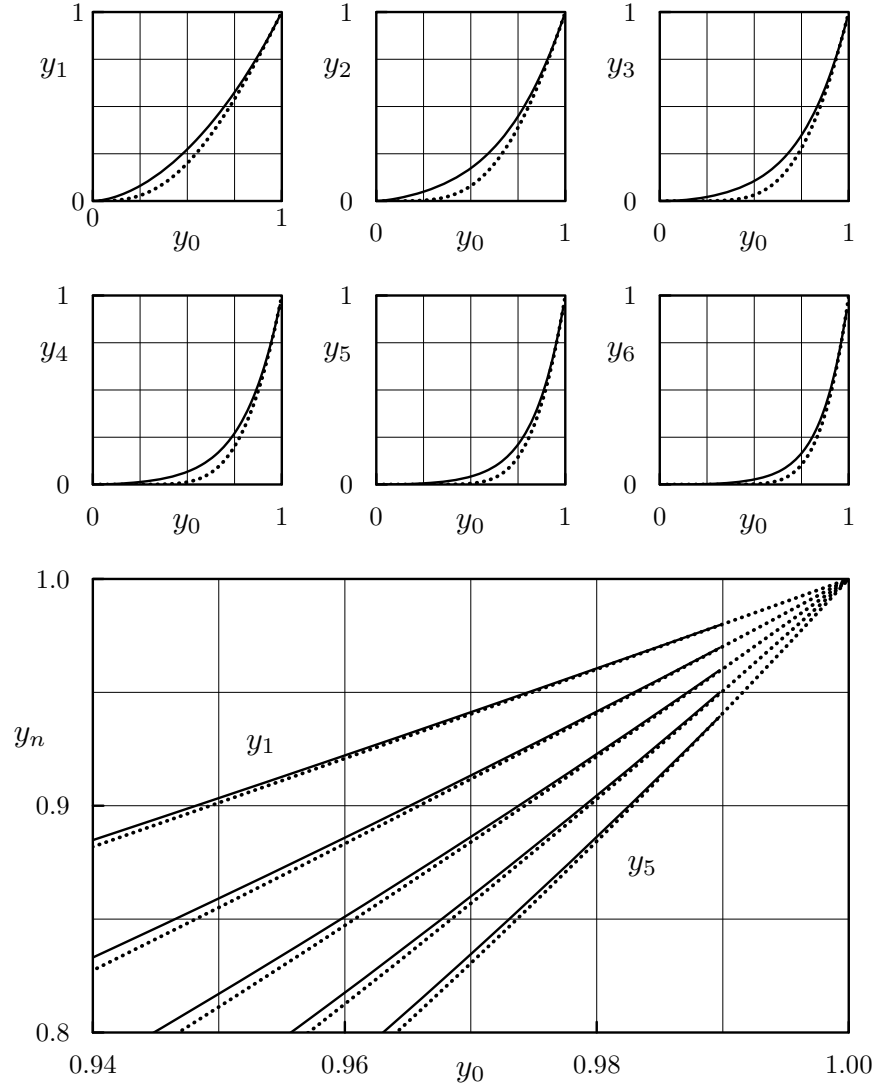


**Fig. 6** Various multipole moments  $y_n$  are plotted versus  $y_0$  for strange matter rings with  $\rho_i/\rho_o = 0.7$  (solid lines) and the sequence of Kerr solutions (dotted lines). In the detailed plot, the curve for  $y_6$  was omitted because of slight numerical inaccuracies for higher multipole moments.

In contrast, we present the multipole moments for configurations near the Newtonian limit ( $e^{-V_0} = 1.1$ ) in Table 2. Here one can see that there is far more variation amongst the rings and that the disc of dust differs significantly from any of the rings. The values in the table also reflect the fact that strange matter has the same Newtonian limit as homogeneous matter.

	$y_0$ ( $\times 10^{-2}$ )	$y_1$ ( $\times 10^{-3}$ )	$y_2$ ( $\times 10^{-3}$ )	$y_3$ ( $\times 10^{-5}$ )	$y_4$ ( $\times 10^{-5}$ )
s.m. ( $r_i/r_o = 0.6$ )	2.22	1.21	1.04	8.92	7.44
s.m. ( $r_i/r_o = 0.7$ )	2.09	1.16	1.02	8.69	7.43
s.m. ( $r_i/r_o = 0.8$ )	1.92	1.09	0.978	8.49	7.46
hom. ( $r_i/r_o = 0.7$ )	2.09	1.16	1.01	8.68	7.42
pol. ( $r_i/r_o = 0.7$ )	2.14	1.27	1.11	10.1	8.75
rel. disc of dust	2.36	1.73	1.56	12.5	21.7

**Table 2** The multipole moments  $y_n$  for various configurations, all with  $e^{-V_0} = 1.1 \Leftrightarrow Z_0 = 0.1$ . The configurations are labelled as in Table 1.

A further comparison of rings of various eos can be found in Fig. 7. Sequences of rings rotating at the mass-shedding limit, are plotted in a two-dimensional parameter space with  $1 - e^{V_0}$  on the  $y$ -axis and  $\rho_i/\rho_o$  on the  $x$ -axis. The mass-shedding limit is reached when the path followed by a particle rotating at the outer edge of the ring becomes a geodesic. For a given eos, other ring configurations (i.e. not rotating at the mass-shedding limit) lie to the right of the corresponding curve. One can see that a transition to the extreme Kerr black hole is a generic feature of all rings considered here. The transition to spheroidal bodies exists for strange matter rings, but not for all eos. What is particularly striking is how close together the curves for strange and homogeneous rings remain right up to the black hole limit. This figure is a modified version of Fig. 1 of [6]. A discussion of the polytropic and Chandrasekhar eos can also be found in that paper.

#### 4 Throat geometry

One of the most interesting features of bodies near the extreme Kerr black hole limit is the appearance of a throat geometry [16, 4]. In the limit, the throat separates the ‘inner world’, containing the ring, from the ‘outer world’. The outer world is the asymptotically flat extreme Kerr spacetime, which is described by a single parameter and in which the horizon is located at the end of the infinitely long throat. On the other hand, the inner world is not asymptotically flat and is related to the outer world through its asymptotic behaviour, which contains information about the one free parameter that uniquely describes the outer world. Any point in the outside world is infinitely far away from any point in the inner world. For example, in the equatorial plane, one finds that the radial proper distance  $\delta$  from the point  $\rho = 0$  to the point  $\rho$  is

$$\delta = \int_0^\rho \sqrt{g_{\rho\rho}}|_{\zeta=0} d\rho. \quad (21)$$

If one measures the proper distance from a point  $\rho_1$  to a point  $\rho$  in the above equation, then it tends logarithmically to  $\infty$  for the extreme Kerr

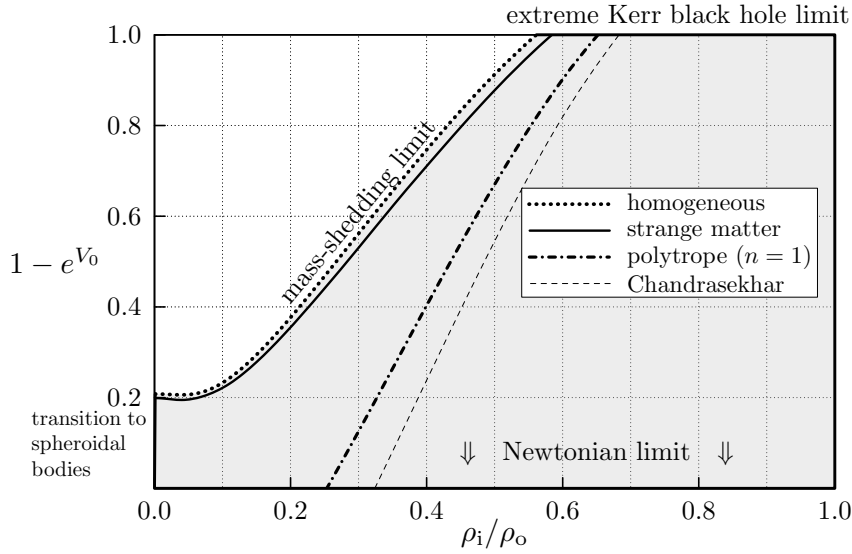


**Fig. 7** The parameter space for rings with a variety of eos is considered in the  $(\rho_i/\rho_o)-(1 - e^{V_0})$  plane. Each eos is bounded on the left by the corresponding mass-shedding curve.

black hole as  $\rho_1 \rightarrow 0$  (the horizon in the coordinates used here is located at  $\rho = 0$ )<sup>2</sup>.

One way to represent the throat is to plot  $\sqrt{g_{\varphi\varphi}}/M$  in the equatorial plane as a function of  $\delta/M$ . Then, the throat appears as a plateau, i.e. a region appears in which the circumference of a circle of constant radius  $\rho = \rho_c$ , tends toward a constant, independent of the radius  $\rho_c$ . As the extreme Kerr black hole is approached, this region becomes infinitely long. Figure 8 shows the appearance of the throat for a sequence of strange matter rings with  $\rho_i/\rho_o = 0.7$  as the parameter  $e^{V_0}$  tends to zero. Even in the first of these pictures ( $e^{2V_0} = 10^{-1}$ ), the highly relativistic nature of the ring is demonstrated by the fact that a small portion of the curve has a negative slope. That is, there exists a region of spacetime in which circles lying in the equatorial plane and centred about the origin have decreasing circumference with increasing radius. The last of these pictures is similar to Fig. 13 in [17] in which the ‘inner world’ is separated from the extreme Kerr solution by the infinite throat region. The proper distance between a point in what becomes the inner world (e.g. the outer edge of the ring  $\rho = \rho_o$ ) and a point in what becomes the outer world (e.g.  $\rho = M$ ) tends to infinity as  $e^{2V_0} \rightarrow 0$ . In a sense, we can say that the ‘throat region’ near the black hole limit

<sup>2</sup> It is thus to be expected that as  $Z_0$  becomes large, the outer coordinate radius of the ring, as measured in units of mass for example, will become small. The shape of the ring itself does not change qualitatively as can be seen in Fig. 3 of [5] which depicts the shape of the ring along a sequence tending to the black hole limit.

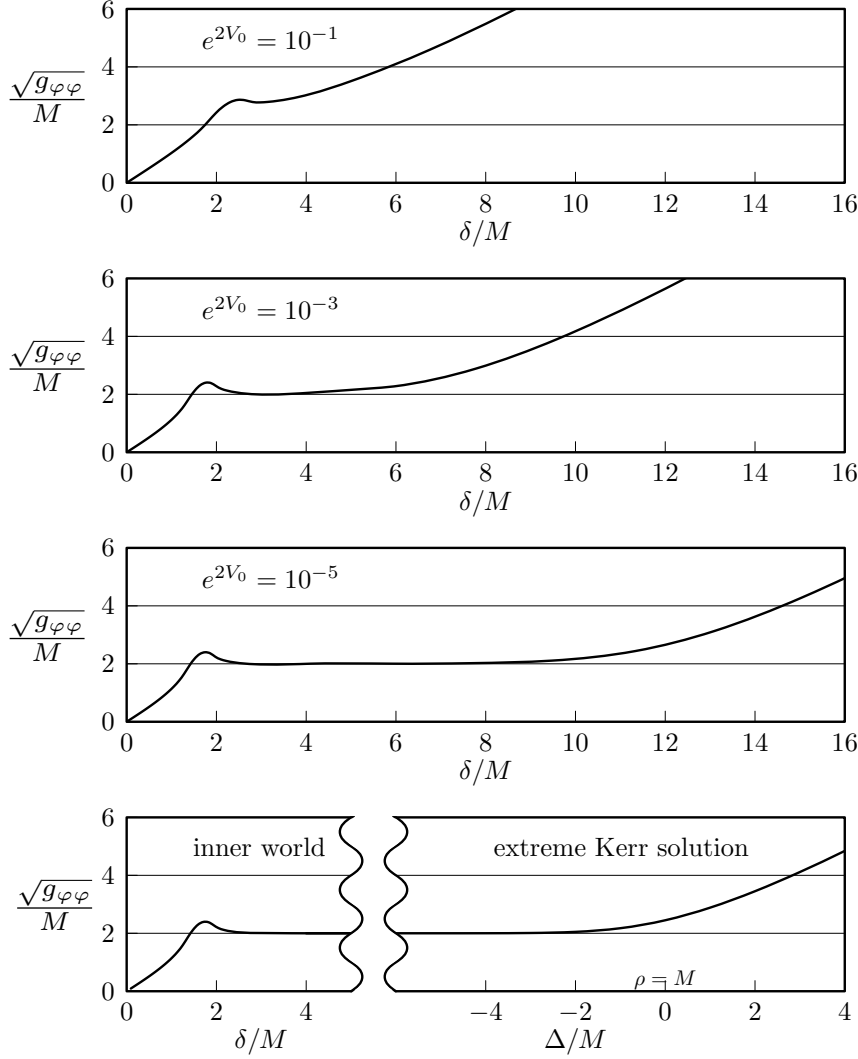


**Fig. 8** The function  $\sqrt{g_{\varphi\varphi}}$  in the equatorial plane is plotted versus proper distance, both normalized with respect to the mass  $M$ . In the throat region,  $\sqrt{g_{\varphi\varphi}}/M$  tends to the constant value 2. All four plots were made for a strange matter ring with a radius ratio  $\rho_i/\rho_o = 0.7$  and with a value for  $e^{2V_0}$  as indicated. In the last plot,  $\Delta$  gives the proper distance in the Kerr metric to the reference point  $\rho = M$ . Note that the proper distance between any point in the ‘inner world’ region and any point in the ‘extreme Kerr’ region tends to infinity as  $e^{2V_0} \rightarrow 0$ .

‘swallows’ the information as to what kind of configuration is sitting at the centre, as can be seen in Table 1.

The numerical ‘inner world’ solution was produced with a program that prescribes the asymptotic behaviour of the throat region (see [16]). Since the ‘asymptotically flat computer program’ is capable of rendering rings with a relative redshift  $Z_0$  well in excess of 100, the metric behaviour provided by this program can be used as initial input for the Newton-Raphson method of the ‘inner world program’ [14]. The fact that such initial data converges to an inner world solution is in itself strong numerical evidence for the existence of a continuous transition to the black hole.

## 5 Escape energy

With the four-velocity  $u^i$  and the Killing vector  $\xi = \partial/\partial t$  corresponding to stationarity, one can define the specific energy of a test particle with respect to infinity, i.e. the energy per unit mass, as

$$E = -u^i \xi_i, \quad (22)$$

which is a conserved quantity along any geodesic.

With  $u^i$  referring to the four-velocity of a particle resting on the ring’s surface,  $E - 1$  could be called the “escape energy”. If it is negative, then a sufficiently small perturbation will not suffice to induce the particle’s escape to infinity on a geodesic, and it is referred to as gravitationally bound. In proving that  $V_0 \rightarrow -\infty$  is a sufficient condition for reaching the Black Hole limit [2], use was made of the reasonable assumption that particles on the fluid’s surface are gravitationally bound. One expects that this minimal requirement for stability will always be satisfied. We now proceed to verify this assumption for a large class of rings.

Figures 9 and 10 show the value of  $E$  along the surface of a variety of strange matter rings as it depends on radius. The radial parameter  $(\rho - \rho_i)/(\rho_o - \rho_i)$  is chosen such that it runs from 0 to 1 for every ring. In Fig. 9 curves are plotted for a constant value  $\rho_i/\rho_o = 0.7$  and for varying  $V_0$ . We see that  $E$  tends to 1 in the Newtonian limit, which follows directly from Eq. (22). Figure 10 shows the behaviour of  $E$  for various values of  $\rho_i/\rho_o$  and constant  $V_0$ . Since configurations with small  $\rho_i/\rho_o$  do not exist when  $V_0$  becomes too negative (see Fig. 7), we chose  $V_0$  to be in the Newtonian regime in order to be able to consider a wide range of values for the radius ratio. For every example considered in Figs 9 and 10, a maximal value at the outside edge of the ring in the equatorial plane is reached, just as one would expect. It is interesting to compare these results with the relativistic disc of dust for which  $E = 1$  holds at the outer edge independent of the value of  $Z_0$  [18].

Focussing our attention now on the outer edge of the ring in the equatorial plane, we see in Fig. 11 how  $E$  depends on  $V_0$  for a sequence of strange matter rings with  $\rho_i/\rho_o = 0.7$ . It is apparent that a maximum is reached

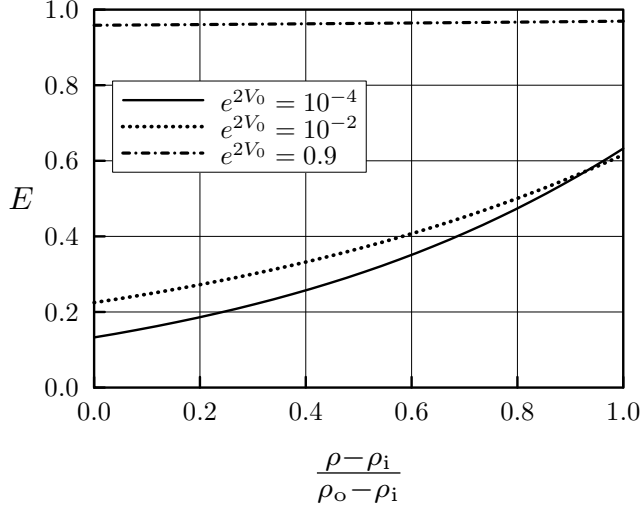


**Fig. 9** The specific energy  $E$  versus  $(\rho - \rho_i)/(\rho_o - \rho_i)$  on the surface of a variety of strange matter rings with  $\rho_i/\rho_o = 0.7$ .

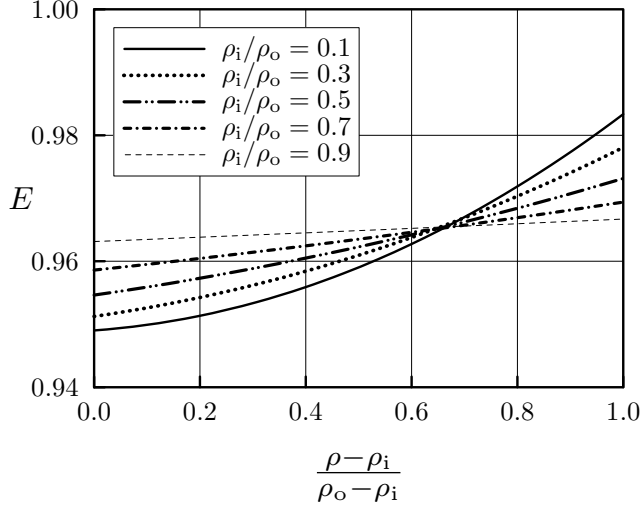


**Fig. 10** The specific energy  $E$  versus  $(\rho - \rho_i)/(\rho_o - \rho_i)$  on the surface of a variety of strange matter rings near the Newtonian limit ( $e^{2V_0} = 0.9$ ).

in the Newtonian limit. For rings rotating at the mass-shedding limit, the value of  $E$  is also significantly smaller than one for small  $e^{V_0}$ . The results for homogeneous rings are very similar and we can verify that  $E \leq 1$  holds (i.e. the escape energy is negative) for a large class of rings.

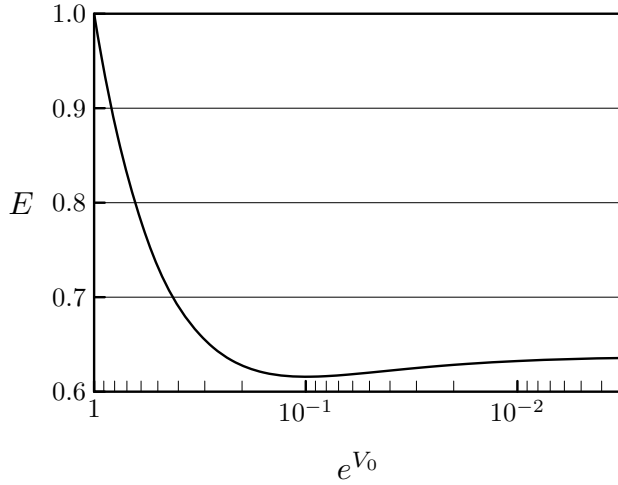


**Fig. 11** The specific energy  $E$  versus  $e^{V_0}$  at the outer edge in the equatorial plane for strange matter rings with  $\rho_i/\rho_o = 0.7$ .

## 6 Summary

It was shown numerically that a parametric transition exists from strange matter rings to the extreme Kerr black hole. Whereas it is known analytically that the eos describing strange matter tends to that of a homogeneous body in the Newtonian limit, it was shown here that properties of configurations with these two eos remain similar right up to the limit  $V_0 \rightarrow -\infty$ .

Figs 1 and 2 suggest that the transition to the black hole is rather slow as  $e^{2V_0} \rightarrow 0$ . This can be made more precise through the comparison with the Kerr solution, which leads us to conjecture that for every stationary rotating body permitting a transition to a black hole, the multipole moments  $y_n$  tend to one according to the formula

$$\frac{dy_n}{dy_0}(y_0 = 1) = n + 1.$$

It is expected that  $E \leq 1$  always holds on the surface of a fluid body. Indeed, this inequality was used to prove that for rotating fluids the extreme Kerr black hole necessarily results if  $e^{2V_0} \rightarrow 0$  [2]. We have verified that this inequality is correct for a large class of rings.

As our knowledge of astrophysical collapse scenarios improves, it will be interesting to see how strong the connections can be to the quasi-stationary collapse considered here.

*Acknowledgements* The authors wish to thank Reinhard Meinel for all his help, Andreas Kleinwächter for providing us with multipoles for the relativistic disc of dust and Stefan Horatschek for many useful discussions. This research was funded in part by the Deutsche Forschungsgemeinschaft (SFB/TR7-B1).

## References

1. R. Meinel. Quasistationary collapse to the extreme Kerr black hole. *Ann. Phys. (Leipzig)*, 13:600, 2004.
2. R. Meinel. On the black hole limit of rotating fluid bodies in equilibrium. *Class. Quantum Grav.*, 23:1359, 2006.
3. G. Neugebauer and R. Meinel. General relativistic gravitational field of a rigidly rotating disk of dust: Solution in terms of ultraelliptic functions. *Phys. Rev. Lett.*, 75:3046, 1995.
4. R. Meinel. Black holes: A physical route to the Kerr metric. *Ann. Phys. (Leipzig)*, 11:509, 2002.
5. M. Ansorg, A. Kleinwächter, and R. Meinel. Relativistic Dyson rings and their black hole limit. *Astrophys. J. Lett.*, 582:L87, 2003.
6. T. Fischer, S. Horatschek, and M. Ansorg. Uniformly rotating rings in general relativity. *Mon. Not. R. Astron. Soc.*, 364:943, 2005.
7. E. Gourgoulhon, P. Haensel, R. Livine, E. Paluch, S. Bonazzola, and J. A. Marck. Fast rotation of strange stars. *Astron. Astrophys.*, 349:851, 1999.
8. M. Ansorg, T. Fischer, A. Kleinwächter, R. Meinel, D. Petroff, and K. Schöbel. Equilibrium configurations of homogeneous fluids in general relativity. *Mon. Not. R. Astron. Soc.*, 355:682, 2004.
9. P. Kordas. Reflection-symmetric, asymptotically flat solutions of the vacuum axisymmetric Einstein equations. *Class. Quantum Grav.*, 12:2037, 1995.
10. R. Meinel and G. Neugebauer. Asymptotically flat solutions to the Ernst equation with reflectional symmetry. *Class. Quantum Grav.*, 12:2045, 1995.
11. R. Geroch. Multipole moments. II. curved space. *J. Math. Phys.*, 11(8):2580, 1970.
12. R. O. Hansen. Multipole moments of stationary space-times. *J. Math. Phys.*, 15(1):46, 1973.
13. G. Fodor, C. Hoenselaers, and Z. Perjés. Multipole moments of axisymmetric systems in relativity. *J. Math. Phys.*, 30(10):2252, 1989.
14. M. Ansorg, A. Kleinwächter, and R. Meinel. Highly accurate calculation of rotating neutron stars: Detailed description of the numerical methods. *Astron. Astrophys.*, 405:711, 2003.
15. A. Kleinwächter, R. Meinel, and G. Neugebauer. The multipole moments of the rigidly rotating disk of dust in general relativity. *Phys. Lett. A*, 200:82, 1995.
16. J. Bardeen and G. T. Horowitz. Extreme Kerr throat geometry: A vacuum analog of  $\text{AdS}_2 \times \text{S}^2$ . *Phys. Rev. D*, 60:104030, 1999.
17. J. M. Bardeen and R. V. Wagoner. Relativistic disks. I. uniform rotation. *Astrophys. J.*, 167:359, 1971.
18. R. Meinel and A. Kleinwächter. Dragging effects near a rigidly rotating disk of dust. In J. B. Barbour and H. Pfister, editors, *Mach's Principle: From Newton's Bucket to Quantum Gravity*, page 339, Boston, 1995. Birkhäuser.